Pyrochlore-supergroup minerals: Potential sinks for toxic elements in aqueous matrices

Alice Taddei
Department of Earth Sciences, University of Firenze, via G. La Pira 4, 50121 Firenze

DOI: 10.19276/plinius.2026.01.019

INTRODUCTION

Minerals belonging to the pyrochlore supergroup and their synthetic analogues have long attracted scientific interest owing to their distinctive chemical and structural features, which allow a range of applications across different fields (Wang et al., 2023, and references therein).

Pyrochlores are oxides of high-charged metals (Nb, Ta, Ti, W) or Sb^{5+}, typically occurring as primary phases in highly evolved, late-stage igneous systems such as carbonatites, granitic pegmatites and nepheline syenites (Lumpkin & Ewing, 1995). Pyrochlore supergroup minerals are characterised by the structural formula $A_{2-m}B_2X_{6-w}Y_{1-n}$, where *m*, *w* and *n* represent structural vacancies (Atencio et al., 2010). The *A* site is 8-fold coordinated and hosts a wide range of cations of different charge and size (Na^+, Ca^{2+}, Sr^{2+}, Ba^{2+}, Pb^{2+}, Y^{3+}, Ce^{3+}, U^{4+}, H_2O, *etc.*), and it can be partially vacant; the *B* site, octahedrally coordinated, usually accommodates Nb, Ta, Ti, W, or Sb^{5+}; *X* is occupied by O or F, but it can be partially vacant or partially occupied by OH^- groups in altered pyrochlores; the *Y* site can host either H_2O molecules, anions (OH^-, F^-, O^{2-}) or large cations (K^+, Cs^+) (Ercit et al., 1993).

The pyrochlore structure (Fig. 1) is generally cubic (space group $Fd\bar{3}m$) and consists of a framework of corner-sharing *B*-site octahedra that forms tunnels along the [110] direction (Atencio et al., 2010). These tunnels host the *A* and *Y* sites and are responsible for many of the peculiar properties of pyrochlores, including their ion-exchange behaviour. In altered pyrochlores, these sites are often partially vacant or occupied by H_2O or, possibly, H_3O^+, highly mobile species which are more likely to be exchanged with large, toxic cations dissolved in aqueous solutions. Where aqueous species are predominant, and thus the tunnel sites are disordered, satellite sites nearby *A* and *Y* can be observed to maintain plausible distances between the atoms (Ercit et al., 1994).

Members of the pyrochlore supergroup and their synthetic analogues are well known for their versatility across a wide spectrum of technological and industrial applications. This flexibility arises from their peculiar crystal structure, and the remarkable variety of chemical species that it can accommodate. Within the scope of this work, the most relevant feature of pyrochlores is their ion-exchange capability, which has the potential to be exploited for environmental remediation applications. Previous studies have shown that pyrochlores may incorporate toxic elements such as Pb or Sb (Han et al., 2014; Radková et al., 2017; Jurkovič et al., 2019), while earlier observations also suggested the possibility of Tl incorporation into hydrated pyrochlores (Jäger et al., 1959; Van Der Veen, 1963; Harris, 1965; Bindi et al., 2006). However, despite the high toxicity and mobil-

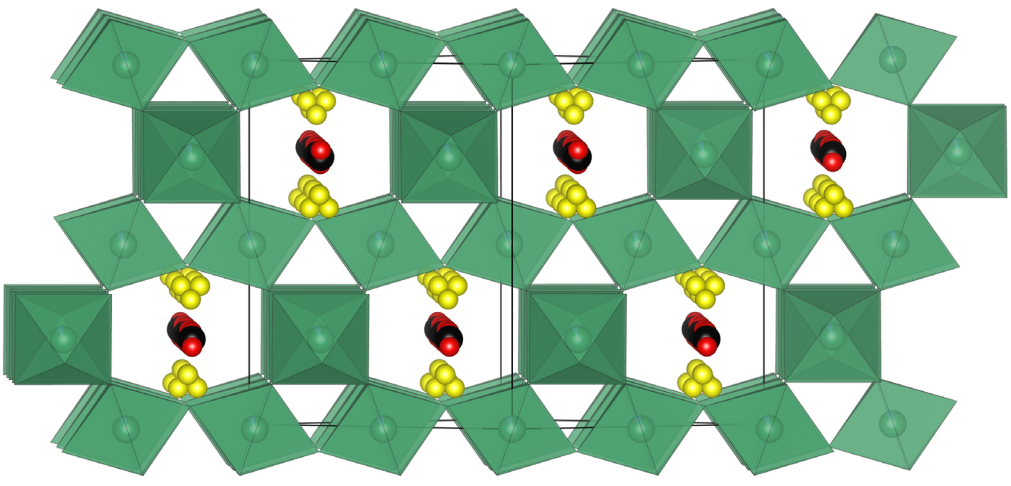

Figure 1 *Pyrochlore structure viewed approximately along [110], showing satellite sites nearby the A and Y sites. Symbols: green octahedra = B, black spheres = A, red spheres = A′, yellow spheres = Y′. The X site is located at the corners of the octahedra, while the Y site would be positioned at the centre of the Y′-centred tetrahedron.*

ity of Tl^+ in aqueous environments, the potential use of natural pyrochlores as sinks for thallium remains poorly explored (Zoppi, 2004). It is thus crucial to further pursue the issue, since pollution from thallium is rapidly becoming a concerning matter due to its high toxicity and enhanced mobility in aqueous solutions, especially when it is present in its reduced state (*e.g.*, Biagioni et al., 2017; George et al., 2019).

Ion-exchange processes may indeed take place at the tunnel sites of pyrochlores, especially when they are occupied by highly mobile species (*e.g.*, H_2O or H_3O^+) or when they are partially vacant, which are common features for natural, strongly weathered species. Defective, hydrated pyrochlores thus represent the most suitable candidates for environmental applications and are thus the species investigated in this work.

METHODS

The studied samples come from several localities worldwide, focusing on hydropyrochlore and hydrokenopyrochlore from Lueshe (D.R. Congo), hydrokenopyrochlore from Araxá (Brazil), and hydrokenomicrolite and kenomicrolite from the Volta Grande pegmatite, Nazareno (Brazil). Additional pyrochlore-supergroup samples from Norway, Russia, Italy, Canada, Sweden, and the United Kingdom were also preliminarily characterised.

Quantitative chemical analyses were performed using a JEOL JXA-8230 electron microprobe operating in wavelength-dispersive spectroscopy (WDS) mode. Analytical data were normalised on the basis of $\Sigma B = 2$ atoms per formula unit.

To investigate ion-exchange processes, imbibition experiments were carried out on both single crystals and polished epoxy mounts. The treatments involved the soaking of pyrochlore samples in water-diluted Clerici solution, as well as in Tl^+- and Pb^{2+}-rich aqueous solutions, having different concentrations, prepared using thallium(I) formate and lead nitrate, respectively. The duration of the experiments ranged from minutes to several days in order to investigate both structural effects and reaction kinetics.

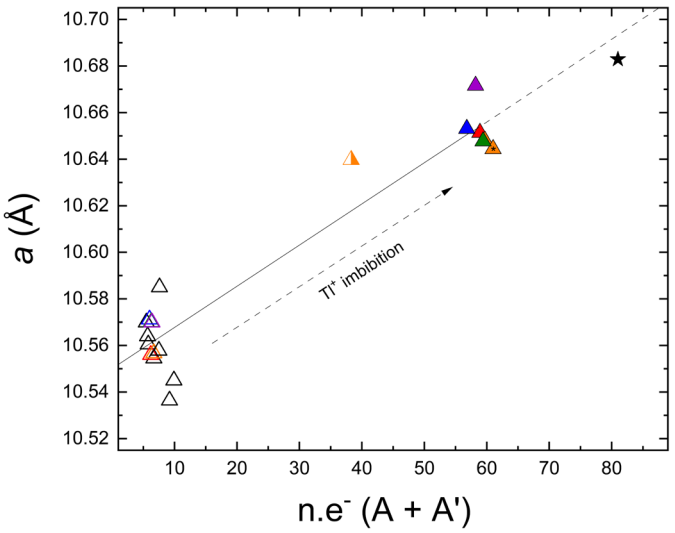

Figure 2 *Unit-cell parameter plotted against the number of electrons at the A and A' sites. Empty and filled symbols represent untreated and Tl-treated, respectively (* denotes the second imbibition in Tl^+-rich solution). The black star symbol indicates $Tl^+_{2-x}Tl^{3+}_xNb_2O_{6+x}$ (x = 0.07) (Fourquet et al., 1995). Regression line (fitting the equation y = 0.0018x + 10.550, R^2 = 0.91) is calculated with samples from this work only.*

Single-crystal X-ray diffraction (SC-XRD) was employed as the main analytical technique to monitor structural modifications induced by the treatments. SC-XRD data were collected both before and after each experiment by means of a Bruker D8 Venture diffractometer equipped with a Photon III detector, using graphite-monochromatized Mo$K\alpha$ radiation (λ = 0.71073 Å). Intensity data were corrected for Lorentz-polarisation effects and for absorption with APEX3 (Bruker, 2016) or APEX5 (Bruker, 2023).

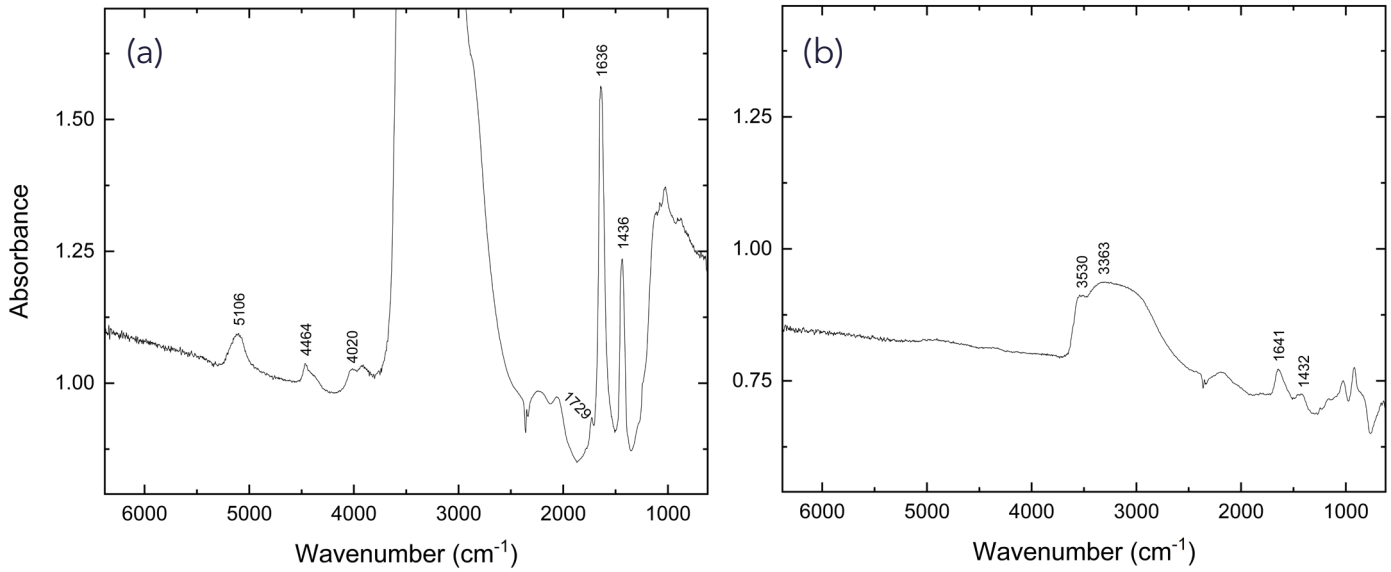

Figure 3 a) *FT-IR spectrum acquired from a small, untreated hydropyrochlore fragment.* ***b)*** *FT-IR spectrum acquired from a Tl-treated hydropyrochlore crystal.*

Additional information on the role of water and hydroxyl groups within the structures was obtained through Fourier-transform infrared spectroscopy (FT-IR). The analyses were carried out with a Bruker Vertex 70 spectrometer attached to a Hyperion 2000 microscope and with a Nicolet iS50 spectrometer attached to a Nicolet RaptIR microscope, on both single crystals and KBr pellets, in transmission mode (MCT detector).

RESULTS

Hydrokenopyrochlore and hydropyrochlore from Lueshe (D.R. Congo)

Hydropyrochlore [ideal formula $(H_2O,□)_2Nb_2(O,OH)_6(H_2O)$] and hydrokenopyrochlore [ideal formula $(□,H_2O)_2Nb_2(O,OH)_6(H_2O)$] from Lueshe show a marked capability to incorporate Tl^+ during imbibition experiments. Structure refinements and chemical analyses indicate that thallium mainly enters the *A* site, replacing an aqueous species (either OH^-+H_2O or H_3O^+). Tl incorporation induces clear structural modifications, such as an expansion of the unit-cell parameter (from 10.536–10.585 Å to 10.644–10.672 Å; Fig. 2) as a consequence of the lengthening of the *A*–*X* bond distance (from 2.719–2.721 Å to 2.761 Å). The expansion is consistent with an increase of electrons (from ~ 6 to ~ 60 e^-) at the *A* site, reaching occupancies corresponding to ~ 70% Tl (~ 1.40 apfu). Following desorption experiments performed in deionized water, the number of electrons at *A* decreases to ~ 38 e^-, suggesting the partially reversible nature of the incorporation reaction.

FT-IR spectra of untreated samples display all the features that indicate the presence of water, with a peak at 1634 cm^{-1} ascribed to H–O–H bending vibrations and a band from 3000 to 3600 cm^{-1} in the O–H stretching mode zone. An unusual peak at 1729 cm^{-1} could point to the occurrence of H_3O^+ in the tunnels (Fig. 3a); this peak is not observed in the spectrum of a Tl-treated sample (Fig. 3b).

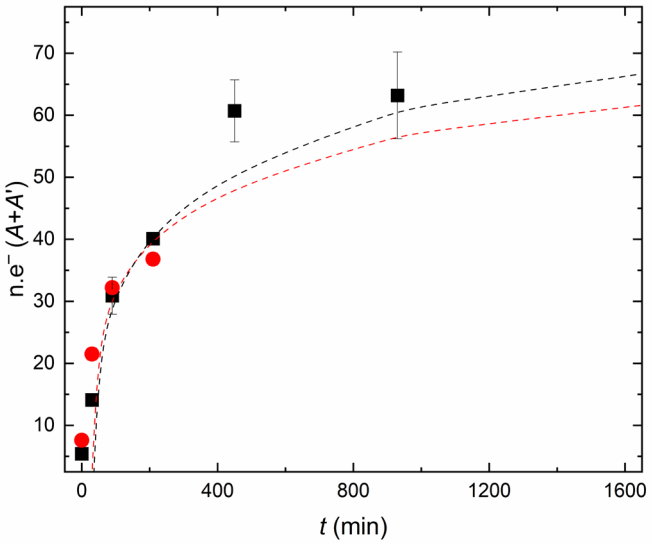

Figure 4 *Number of electrons at A+A′ plotted against time of imbibition. The points of both datasets (black squares: sample imbibed in a 1M Tl solution; red circles: sample imbibed in a 0.1M Tl solution; empty symbols are untreated samples) are approximated by a logarithmic curve. Data collected at t = 0 were not considered for the calculation of the curves. The black dashed line can be expressed as y = 15.107ln(x) – 37.339 (R^2 = 0.96), while the red dashed line can be expressed as y = 10.681ln(x) – 16.396 (R^2 = 0.98). The error bars relative to n.e⁻ (A+A′) that are not visible are contained within the data symbols.*

Experiments aimed to evaluate the Tl-incorporation reaction kinetics indicate that the process is relatively rapid and follows logarithmic trends typical of exchange reactions (Fig. 4). Most structural changes occur, in fact, within the first hours of treatment, reaching a plateau after only eight hours. In short imbibition experiments, Tl enters both *Y′* and *A*, progressively ordering at *A* for longer experimental durations.

Hydrokenopyrochlore from Araxá (Brazil)

In hydrokenopyrochlore from Araxá Tl incorporation was also observed, although the reaction kinetics is slower and the structural response is less pronounced compared to the Lueshe samples (*e.g.*, the increase unit-cell parameter *a* is less dramatic, changing from 10.53–10.56 Å to 10.56–10.63 Å).

The higher Ba content of the Araxá samples appears to play an important role in controlling the exchange mechanism. In this case, Tl incorporation likely involves exchange processes with Ba^{2+}, which are less efficient than those involving tunnel sites hosting aqueous species, as the maximum number of electrons observed at *A* (~ 39 e^-) converts to, roughly, 0.54 Tl^+ pfu. Consequently, the structural variations associated with Tl uptake follow trends different from those observed in hydropyrochlore from Lueshe (Fig. 5). Pb imbibition experiments, instead, produced nearly no effects, indicating a limited (if any) Pb-incorporation phenomenon.

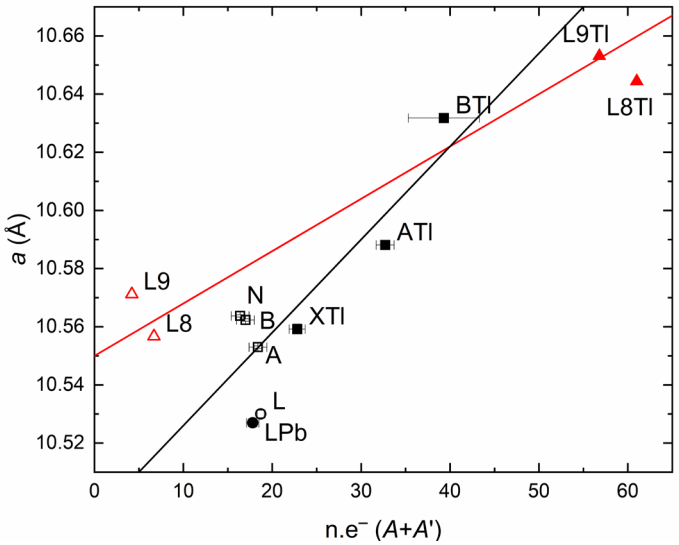

Figure 5 *Number of electrons at the A+A′ sites plotted against the unit-cell parameter. Symbols: red triangles are from Taddei et al. (2024); black squares are untreated and Tl-treated samples; black circles represent the untreated and Pb-treated samples. Empty symbols indicate untreated samples, full symbols indicate treated samples. The rate of expansion of the unit cell differs between the two sets of samples probably due to the different composition at the A+A′ sites before the treatments. The red line fits the equation y = 0.0018x + 10.550 (R^2 = 0.91) reported by Taddei et al. (2024), while the black line fits y = 0.0032x + 10.494 (R^2 = 0.78), calculated using the data from this work.*

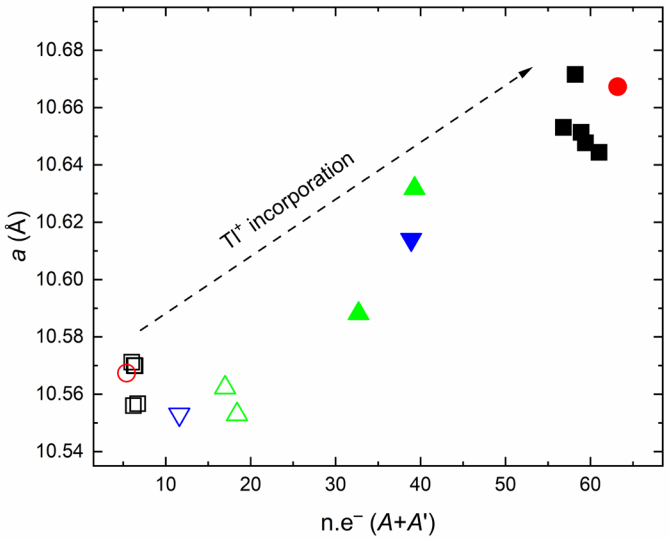

Figure 6 *Unit-cell parameter against the number of electrons refined at A+A' in different pyrochlore samples before and after imbibition in a Tl-rich solution. Symbols: blue, downward triangle = hydrokenomicrolite; green, upward triangle = hydrokenopyrochlore; black squares = hydrokenopyrochlore and hydropyrochlore (data from Taddei et al., 2024); red circles = hydrokenopyrochlore (data from Taddei & Bindi, 2026); empty symbols = untreated samples; filled symbols = Tl-treated samples.*

Hydrokenomicrolite and Kenomicrolite from Nazareno, Minas Gerais (Brazil)

Hydrokenomicrolite [ideal formula $(\square,H_2O)_2Ta_2(O,OH)_6(H_2O)$] from Nazareno also showed the ability to incorporate Tl^+, accompanied by unit-cell expansion (from 10.553 to 10.614 Å) and variations in *A*-site electron density (from ~12 to ~39 e^-) analogous to those observed in other hydrated, defective pyrochlore-group minerals (Fig. 6), incorporating up to ~ 0.68 Tl^+ pfu.

The detailed investigation of these samples led to the identification and characterisation of kenomicrolite [ideal formula $\square_2Ta_2(O,OH)_6\square$, a new member of the microlite group. The mineral revealed a highly defective structure, and it is the first pyrochlore-supergroup member dominated by vacancies at both tunnel sites. Despite its structural similarity to hydrokenomicrolite, kenomicrolite exhibited very limited ion-exchange capability (incorporated Tl^+ up to ~ 0.19 apfu). This behaviour is mainly related to the lack of aqueous species within the tunnels (< 0.35 molecules pfu), highlighting the fundamental role of water in controlling exchange reactions in pyrochlore-supergroup minerals and indirectly pointing to the occurrence of the hydronium ion in these minerals.

DISCUSSION

The results obtained in this work demonstrate that defective and hydrous pyrochlore-supergroup minerals can effectively act as sinks for toxic heavy metals dispersed in aqueous matrices. Their ion-exchange behaviour is strongly controlled by the presence of vacancies and mobile species within the tunnel sites, which facilitate the incorporation of large cations such as Tl^+.

Among the investigated samples, hydropyrochlore and hydrokenopyrochlore from Lueshe showed the highest ion-exchange efficiency. They are characterised by abundant H_2O and/or H_3O^+ species hosted within the tunnels, which appear to be directly involved in the exchange mechanisms. The octahedral framework, on the other hand, remains substantially stable during ion exchange, undergoing only small distortions necessary to accommodate considerable amounts of a large cation such as monovalent thallium. Additionally, the extremely rapid kinetics of the reaction make these species the most promising candidates as sinks for heavy metal among the minerals here studied.

The different behaviour observed in the Araxá samples further emphasises the importance of the initial crystal-chemical features in controlling ion-exchange mechanisms. Tunnel sites enriched in (although not dominated) relatively immobile divalent cations such as Ba^{2+} seem less favourable for rapid incorporation processes compared to phases that are highly hydrated.

The discovery of kenomicrolite furthermore contributes to the knowledge of the pyrochlore supergroup; at the same time, its limited ion-exchange capacity highlights that structural vacancies alone are insufficient to guarantee effective ion exchange if mobile tunnel species are absent (thus indicating, albeit indirectly, more strongly the possible presence of H_3O^+).

The proposed ion-exchange reactions for thallium incorporation are the following:

$$^{A+A'}Ba^{2+} + {}^{Y'}H_2O \rightleftarrows {}^{A+A'}Tl^{+} + {}^{Y'}Tl^{+} \quad (i)$$

$$^{A}\square + {}^{A'+Y'}H_2O + {}^{X}OH^{-} \rightleftarrows {}^{A}Tl^{+} + {}^{A'+Y'}\square + {}^{X}O^{2-} \quad (ii)$$

$$^{A}\square + {}^{A'+Y'}H_3O^{+} + {}^{X}O^{2-} \rightleftarrows {}^{A}Tl^{+} + {}^{A'+Y'}\square + {}^{X}O^{2-} \quad (iii)$$

where reaction (i) applies to Ba-bearing hydrokenopyrochlore, while reactions (ii) and (iii) potentially apply to all the other investigated pyrochlores.

CONCLUSIONS

This study provides a detailed investigation of the crystal chemistry and ion-exchange properties of selected pyrochlore-supergroup minerals, with particular focus on altered, hydrated and defective species, which are seemingly more suitable candidates for remediation purposes.

The results demonstrate that these pyrochlores are capable of incorporating significant amounts of monovalent thallium via ion-exchange mechanisms involving H_2O+OH^- or H_3O^+ species hosted at the tunnel sites. Tl incorporation induces measurable structural modifications, including unit-cell expansion and variations in bond distances and angles, while the octahedral framework only undergoes minor changes due to the enlargement of the *A* polyhedron.

Overall, not only does this work improve the understanding of the ion-exchange behaviour of pyrochlore-supergroup minerals, but it also highlights their potential relevance in environmental applications such as toxic-metal sequestration in aqueous systems. The obtained results also provide useful crystal-chemical insight for the future development of synthetic pyrochlore-type materials for environmental remediation purposes.

REFERENCES

Atencio, D., Andrade, M.B., Christy, A.G., Giere, R., Kartashov, P.M. (2010) - The pyrochlore supergroup of minerals: Nomenclature. The Can. Mineral., 48, 673–698.

Biagioni, C., D'Orazio, M., Lepore, G.O., d'Acapito, F., Vezzoni, S. (2017) - Thallium-rich rust scales in drinkable water distribution systems: A case study from northern Tuscany, Italy. Sci. Total Environ., 587–588, 491–501.

Bindi, L., Petříček, V., Withers, R.L., Zoppi, M., Bonazzi, P. (2006) - A novel high-temperature commensurate superstructure in a natural bariopyrochlore: A structural study by means of a multiphase crystal structure refinement. J. Solid State Chem., 179, 729–738.

Bruker (2016) - APEX3, SAINT and SADABS. Bruker AXS Inc. Madison, WI, USA.

Bruker (2023) - APEX5 v2023. 9-2, SAINT V8. 40B. Bruker AXS Inc. Madison, WI, USA.

Ercit, T.S., Černý, P., Hawthorne, F.C. (1993) - Cesstibtantite—a geologic introduction to the inverse pyrochlores. Miner. Petrol., 48, 235–255.

Ercit, T.S., Hawthorne, F.C., Cerny, P. (1994) - The structural chemistry of kalipyrochlore, a "hydropyrochlore." Can. Mineral., 32, 415–420.

Fourquet, J.L., Duroy, H., Lacorre, Ph. (1995) - $Tl_2Nb_2O_{6+x}$ ($0 \leq x \leq 1$): A Continuous Cubic Pyrochlore Type Solid Solution. J. Solid State Chem., 114, 575–584.

George, L.L., Biagioni, C., Lepore, G.O., Lacalamita, M., Agrosì, G., Capitani, G.C., Bonaccorsi, E., d'Acapito, F. (2019) - The speciation of thallium in (Tl,-Sb,As)-rich pyrite. Ore Geol. Rev., 107, 364–380.

Han, Y.N., Jiao, S., Xu, M., Pang, G., Feng, S. (2014) - Solvothermal synthesis of the defect pyrochlore $KNbWO_6 \cdot H_2O$ and its application in Pb^{2+} removal. RSC Adv., 4, 14357.

Harris, P.M. (1965) - Pandaite from the Mrima Hill niobium deposit (Kenya). Mineral. Mag., 35, 277–290.

Jäger, E., Niggli, E., Van Der Veen, A.H. (1959) - A hydrated barium-strontium pyrochlore in a biotite rock from Panda Hill, Tanganyika. Mineral. Mag., 32, 10–25.

Jurkovič, Ľ., Majzlan, J., Hiller, E., Klimko, T., Volekoá-Lalinská, B., Méres, Š., Göttlicher, J., Steininger, R. (2019) - Natural attenuation of antimony and arsenic in soils at the abandoned Sb-deposit Poproč, Slovakia. Environ. Earth Sci., 78, 672.

Lumpkin, G.R. & Ewing, R.C. (1995) - Geochemical alteration of pyrochlore group minerals; pyrochlore subgroup. Am. Mineral., 80, 732–743.

Radková, A.B., Jamieson, H., Lalinská-Voleková, B., Majzlan, J., Števko, M., Chovan, M. (2017) - Mineralogical controls on antimony and arsenic mobility during tetrahedrite-tennantite weathering at historic mine sites Špania Dolina-Piesky and Ľubietová-Svätodušná, Slovakia. Am. Mineral., 102, 1091–1100.

Taddei, A. & Bindi, L. (2026) Exploring the kinetics of monovalent thallium incorporation in hydropyrochlore and hydrokenopyrochlore. Mineral. Mag., 90, 324–331.

Taddei, A., Bindi, L., Lepore, G.O., Skogby, H., Bonazzi, P. (2024) - Crystallographic insights into monovalent thallium incorporation: Exploring hydropyrochlore structure for environmental remediation. Am. Mineral., 109, 1913–1920.

Van Der Veen, A.H. (1963) A study of Pyrochlore. PhD thesis, Leiden, Verh. K. Ned. Geol. Mijnbouwkd Gen., Geol. Ser. 22, 188 pp.

Wang, Y., Jing, C., Ding, Z.Y., Zhang, Y.Z., Wei, T., Ouyang, J.H., Liu, Z.G., Wang, Y.J., Wang, Y.M. (2023) - The Structure, Property, and Ion Irradiation Effects of Pyrochlores: A Comprehensive Review. Crystals, 13, 143.

Zoppi, M. (2004) - Ossidi di Nb, Ta e Ti: processi di ricristallizzazione e relazioni cristallochimiche. PhD thesis, Università degli Studi di Firenze, Firenze, 166 pp.